Biosensors and Bioelectronics 181 (2021) 113151

Contents lists available at ScienceDirect

Biosensors and Bioelectronics

journal homepage: http://www.elsevier.com/locate/bios

Application of sulfur-doped graphene quantum dots@gold-carbon nanosphere for electrical pulse-induced impedimetric detection of glioma cells

Akhilesh Babu Ganganboina [a], Naresh Kumar Dega [c], Hai Linh Tran [c], Win Darmonto [d], Ruey-An Doong [b,d,*]

[a] Research Institute of Green Science and Technology, Shizuoka University, Shizuoka, Japan
[b] Institute of Analytical and Environmental Sciences, National Tsing Hua University, 101, Sec. 2, Kuang Fu Road, Hsinchu, 30013, Taiwan
[c] Department of Biomedical Engineering and Environmental Sciences, National Tsing Hua University, 101, Sec. 2, Kuang Fu Road, Hsinchu, 30013, Taiwan
[d] Department of Biology, Faculty of Science and Technology, Airlangga University, Surabaya, 60115, Indonesia

ARTICLE INFO

Keywords:
Glioma cells
Impedance
Electric pulse
Angiopep-2 peptide
Graphene quantum dots
Gold decorated carbon nanosphere (Au–CNS)

ABSTRACT

Glioma is the predominant brain tumor with high death rate. The successful development of biosensor to achieve an efficient detection of glioma cells at low concentration remains a great challenge for the personalized glioma therapy. Herein, an ultrasensitive pulse induced electrochemically impedimetric biosensor for glioma cells detection has been successfully fabricated. The 4–11 nm sulfur-doped graphene quantum dots (S-GQDs) are homogeneously deposited onto gold nanoparticles decorated carbon nanospheres (Au–CNS) by Au-thiol linkage to form S-GQDs@Au–CNS nanocomposite which acts as dual functional probe for enhancing the electrochemical activity as well as conjugating the angiopep-2 (Ang-2) for glioma cell detection. Moreover, the application of an externally electrical pulse at +0.6 V expend the surface of glioma cells to accelerate the attachment of glioma cells onto the Ang-2-conjugated S-GQDs@Au–CNS nanocomposite, resulting in the enhanced sensitivity toward glioma cell detection. An ultrasensitive impedimetric detection of glioma cells with a wide linear range of 100–100,000 cells mL^{-1} and a limit of detection of 40 cells mL^{-1} is observed. Moreover, the superior selectivity with long-term stability of the developed biosensor in human serum matrix corroborates the feasibility of using S-GQDs@Au–CNS based nanomaterials as the promising sensing probe for practical application to facilitate the ultrasensitive and highly selective detection of cancer cells.

1. Introduction

Glioblastoma multiforme (GBM) is a rapid-proliferated glioma cell which is well-known for its extreme malignancy as the brain tumor with high lethality and poor prognosis (Wang et al., 2014; Yang et al., 2020). Despite the advance in neuroimaging, neurosurgery, and chemotherapy, the prognosis of GBM is still dismal, primarily due to the recurrence of tumors that are resistant to radiotherapy and chemotherapy treatments (Hu et al., 2020). Due to the dismal prognosis on the GBM cases and its re-emerging prominence resistance to radiotherapy and chemotherapy treatments, a reliable prediction and forecasting method on the GBM is being under huge demand (Tom et al., 2019; Wang et al., 2020b). In addition, the highly migratory and invasive nature of a self-renewing subset of the heterogeneous tumor cell population is mainly attributed to the recurrence of glioma tumors (Chowdhury et al., 2018b; Prager et al., 2020). In addition to the exploitation of the effective treatments for brain tumors as well as tracking of recurrence of glioma tumors, the development of a rapid and selective strategy for glioma cell detection is of great importance. Thus, there is a pressing need to develop a highly sensitive and selective biosensor for glioma cells detection in which individual glioma cells can produce a quantitative signal.

Several devices and techniques have recently been employed as the promising multiplexed tools for highly sensitive detection of cancer biomarkers (Bidram et al., 2019). Some drug delivery vehicles can be linked with peptide ligands to deliver drugs across the blood brain barrier to reach the target tumor cells of interest in brain (Khongkow et al., 2019). In particular, angiopep-2 peptide (Ang-2), with length around 19 amino acids, can recognize and attach to the low-density

* Corresponding author. Institute of Analytical and Environmental Sciences, National Tsing Hua University, Hsinchu, 30013, Taiwan.
E-mail address: radoong@mx.nthu.edu.tw (R.-A. Doong).

https://doi.org/10.1016/j.bios.2021.113151
Received 23 November 2020; Received in revised form 10 February 2021; Accepted 4 March 2021
Available online 10 March 2021

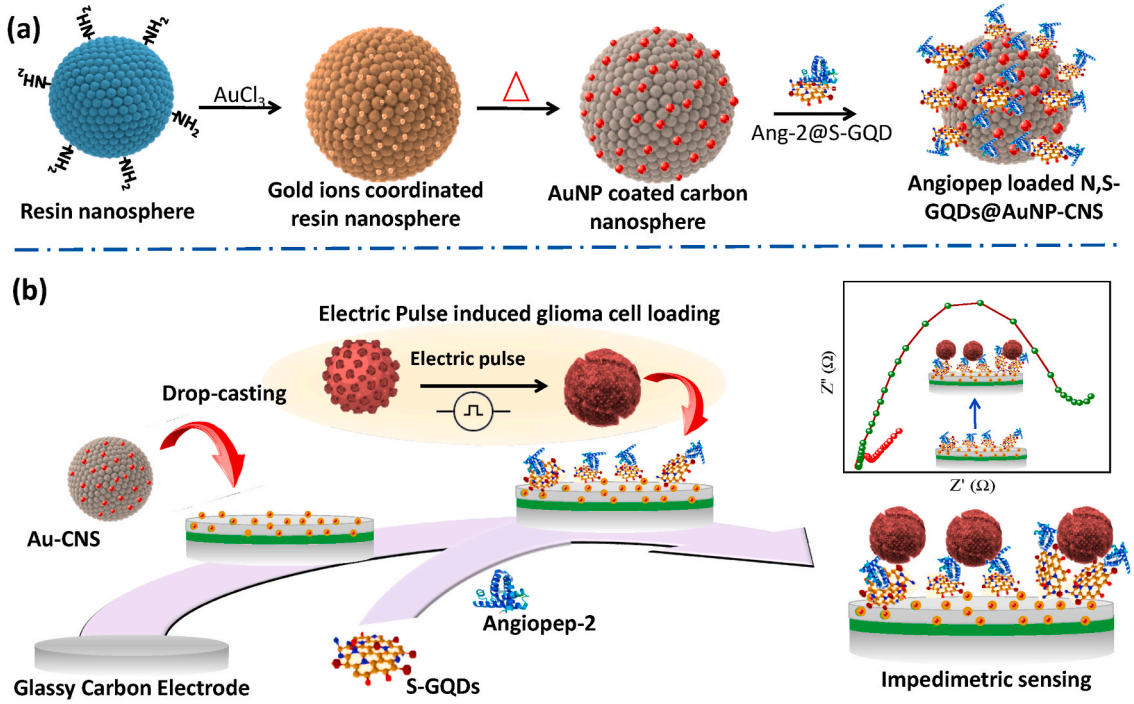

Scheme 1. Illustration of the (a) synthesis and fabrication of GCE||Au–CNS@S-GQD/Ang-2 biosensor and (b) pulse induced electrochemical detection of glioma cells.

lipoprotein receptor protein 1 (LRP1) (Wang et al., 2020a). Since LRP1 receptors are abundantly expressed only in the glioma and endothelial cells compared to the normal brain parenchyma (Huang et al., 2011), Ang-2 can uniquely distinguish and selectively determine the cancer cells to the normal cells as well as deliver the drug delivery vehicles to brain tumor. Therefore, the precise affinity of Ang-2 toward LRP1 receptor of glioma cells can serve as the highly selective probe for GBM detection applications.

Recent progress in fabrication of hybrid nanocomposites has improved the sensing methodology as well as facilitated the development of advanced prospects for electrochemical detection (Li et al., 2020; Song et al., 2020; Wang et al., 2019). In pursuit of ultrasensitive and robust detection performance, studies have emphasized the fabrication of superior nanostructured platform which can load maximum quantity of analytes for superior performance and specificity (Ganganboina et al., 2020; Ganganboina and Doong 2018b; Mansuriya and Altintas 2020). Due to their excellent control of the morphology and microstructure, carbon nanospheres (CNS) have received considerable attention. In addition, CNS has long-term stability and provides pathways to impact the interactions between matrix and nanoparticles (Kumar et al., 2019; Yang et al., 2014). Gold nanoparticle (AuNP) with controlled shapes and excellent properties has proven to be an attractive nanomaterial for highly sensitive detection of biomolecules (Dutta Chowdhury et al., 2018). Therefore, the fabrication of Au–CNS nanocomposite as the potential matrix is an effective strategy to sensitively and selectively detect glioma cells.

Recently, graphene quantum dots (GQDs) have been extensively explored in biomedical fields (Ganganboina and Doong 2020; Ganganboina et al., 2017b). GQDs in various sizes, morphologies and dopants have been developed with promising optical and electrochemical properties to sensitively and selectively detect target anlaytes (Ahmadi et al., 2020; Miao et al., 2019; Xue et al., 2020). For instance, the sulfur-doped GQDs (S-GQDs) can provide anchoring sites for the attachment of AuNP and the carboxylic groups on the edges allow the conjugation of biomolecules onto S-GQDs. It is known that the Ang-2 is a peptide which can covalently conjugate with S-GQDs, this gives an impetus to fabricate the nanocomposite by combining the AuNPs, CNS, and S-GQDs (S-GQDs@Au–CNS) hybrid, which may attain the simultaneous benefits of inorganic and organic constituents, for glioma cells identification in human serum. However, the fabrication of S-GQDs@Au–CNS hybrid materials for electrochemical detection of glioma cells has not been reported yet.

Herein, we have developed a pulse induced impedimetric sensor for ultrasensitive glioma cells detection. The Ang-2 conjugated S-GQDs@Au–CNS is deposited onto glass carbon electrode (GCE) to form an Ang-2/S-GQDs@Au–CNS||GCE sensor, and the glioma cells are detected by impedimetric response using EIS measurement. As illustrated in Scheme 1, the detection of glioma cell is based on the change in impedance of Ang-2/S-GQDs@Au–CNS electrode after attachment of glioma cells. The CNS has a dominant role in acting as a nanocarrier for AuNP development, while the uniform distribution of AuNPs on the CNS surface provides numerous active sites for the successful attachment of S-GQDs by Au-thiol linkage. In addition, the S-GQDs on the S-GQDs@Au–CNS nanocomposite serve as the conjugator for the immobilization of Ang-2. Therefore, the GQDs@Au–CNS nanocomposite can serve as a dual functional probe for enhancing the electrochemical activity as well as conjugating the Ang-2 for glioma cell detection because the non-conducting glioma cells may restrict the electron transfer after the formation of glioma cells–angiopep bioconjugate on the surface of S-GQDs@Au–CNS. Moreover, a new approach by applying various external pulses is examined during the glioma cells attachment process, and electric pulse of +0.6 V shows a superior impedimetric response. The proposed Ang-2/S-GQDs@Au–CNS biosensor performs excellently to detect glioma cells with low detection limit and excellent linearity because of the excellent architecture, good conductivity and fast pulse-induced impedimetric response. Moreover, the excellent selectivity of the proposed Ang-2/S-GQDs@Au–CNS||GCE sensor is conducted, and the detection of glioma cells using human serum as the matrix confirms its practical applicability.

2. Materials and methods

2.1. Chemicals

Citric acid, 3-mercaptopropionic acid, gold (III) chloride trihydrate ($HAuCl_4 \cdot 3H_2O$), Pluronic F127, cysteine, hexadecyltrimethylammonium bromide, resorcinol, 3-aminophenol, ammonium hydroxide solution, N-(3 (dimethylamino)-propyl)-N′-ethyl-carbodiimide hydrochloride (EDC), N-hydroxysuccinimide (NHS) and formaldehyde were purchased from Sigma-Aldrich. Angiopep-2 peptide was obtained from NavoPro. Milli-Q deionized water (18.2 MΩ cm) was used to prepare all the solutions unless otherwise specified.

2.2. Synthesis of AuNP decorated carbon nanospheres (Au@CNS)

The AuNP decorated carbon nanospheres (Au–CNS) were synthesized by a two-stage method. The CNS was first prepared by adding 650 mg CTAB, 500 mg cysteine, and 500 mg pluronic F127 to the well-mixing water/alcohol solution containing 100 mL of distilled water and 40 mL of ethanol. In addition, 1 g of 3-aminophenol was added and stirred vigorously until the complete dissolution. 1.4 mL of formaldehyde was added to the above mixture and stirred for additional 24 h. Furthermore, the mixture was heated up to 100 °C for another 24 h followed by the centrifugation and washing with ethanol and deionized water in sequence, and then dried at 40 °C for 12 h to collect the product.

Afterward, 100 mg as-obtained powder was reacted with 10 mL of 10 mM $HAuCl_4$ under ultrasonication for 10 min and the solution was incubated and stirred for 24 h to fabricate Au@resin nanospheres. Thereupon, the solution was centrifuged and dried overnight at room temperature. The obtained samples were heated up to 700 °C at a rate of 1 °C min^{-1} and maintained for 4 h in N_2 for carbonization to obtain AuNP decorated carbon spheres (Au–CNS).

2.3. Synthesis of S-GQDs@AuNP decorated CNS

S-GQDs were hydrothermally synthesized according to our previous report using pyrolysis method (Anh and Doong, 2018). The as-synthesized S-GQDs were added excessively to the re-dispersed Au–CNS solution and incubated for 24 h under well agitation conditions to maximize the Au-thiol interaction between S-GQDs and the AuNPs in Au–CNS nanocomposites. Finally, deionized water was added and centrifuged to separate the S-GQDs@Au–CNS from unbound S-GQDs, and dried at 60 °C to obtain S-GQDs@Au–CNS.

2.4. Synthesis of Angiopep-2 conjugated S-GQDs@Au–CNS

The biosensing capability of S-GQD@Au–CNS toward the glioma cells detection was selectively defined by the conjugation of Ang-2 on the surface of nanocomposites via the covalent bonding. Briefly, S-GQDs@Au–CNS was added into the EDC/NHS solution for 1 h and then 10 μg mL^{-1} Ang-2 peptide was further added to establish the chemical bonding between the carboxylic moieties of S-GQDs and the cysteine terminal of Ang-2. The excess EDC and NHS were removed by using 1 kDa dialysis bag dialysis, and the purified solution of Ang-2 conjugated S-GQDs@Au–CNS nanocomposite (Ang-2/S-GQDs@Au–CNS) was then stored at 4 °C.

2.5. Characterization of S-GQDs@Au–CNS

The surface characterization of S-GQDs@Au–CNS nanocomposite, including transmission electron microscopy (TEM), X-ray photoelectron spectroscopy (XPS), X-ray diffraction (XRD), and thermal gravimetric analysis (TGA), were performed as described in our previous work (Ganganboina and Doong 2019). Briefly, the size and shape of S-GQDs@Au–CNS were identified with JOEL high resolution TEM (HRTEM) at 200 kV. Bruker D8 Advance X-ray diffractometer with Ni filtered Cu Kα radiation (λ = 1.5406 Å) and Mettler Toledo DSC/TGA 3+ Stare system were used to identify the crystallinity and thermal property of S-GQDs@Au–CNS, respectively. Moreover, an ESCA Ulvac-PHI 1600 X-ray photoelectron spectrometer from Physical Electronics using Al-Kα radiation photon energy at 1486 ± 0.2 eV was used to examine the change in chemical species of elements in S-GQD@Au–CNS.

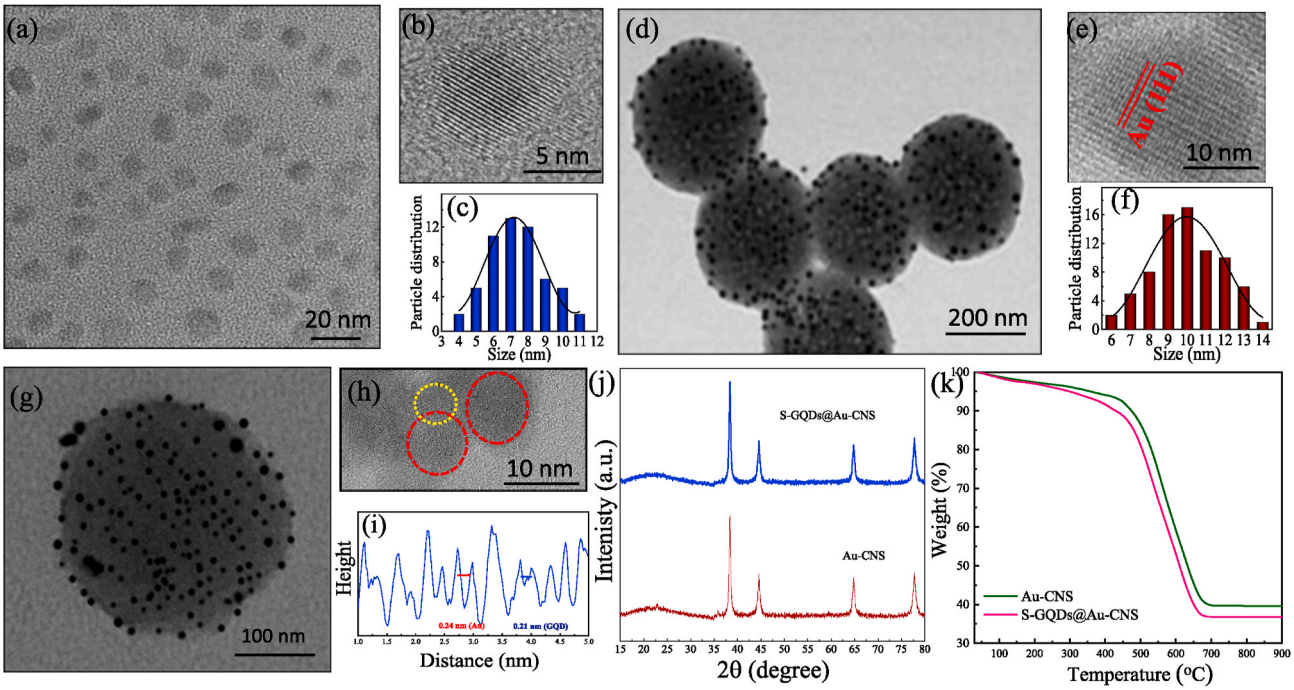

Fig. 1. The (a) TEM and (b) HRTEM images, and (c) particle size distribution of S-GQDs, (d) TEM and (e) HR-TEM images, and (f) particle size distribution of Au–CNS, (g) TEM and (h) HR-TEM images, and (i) lattice pattern of S-GQDs@Au–CNS, (j) XRD patterns, and (k) thermal properties of Au–CNS based nanocomposites.

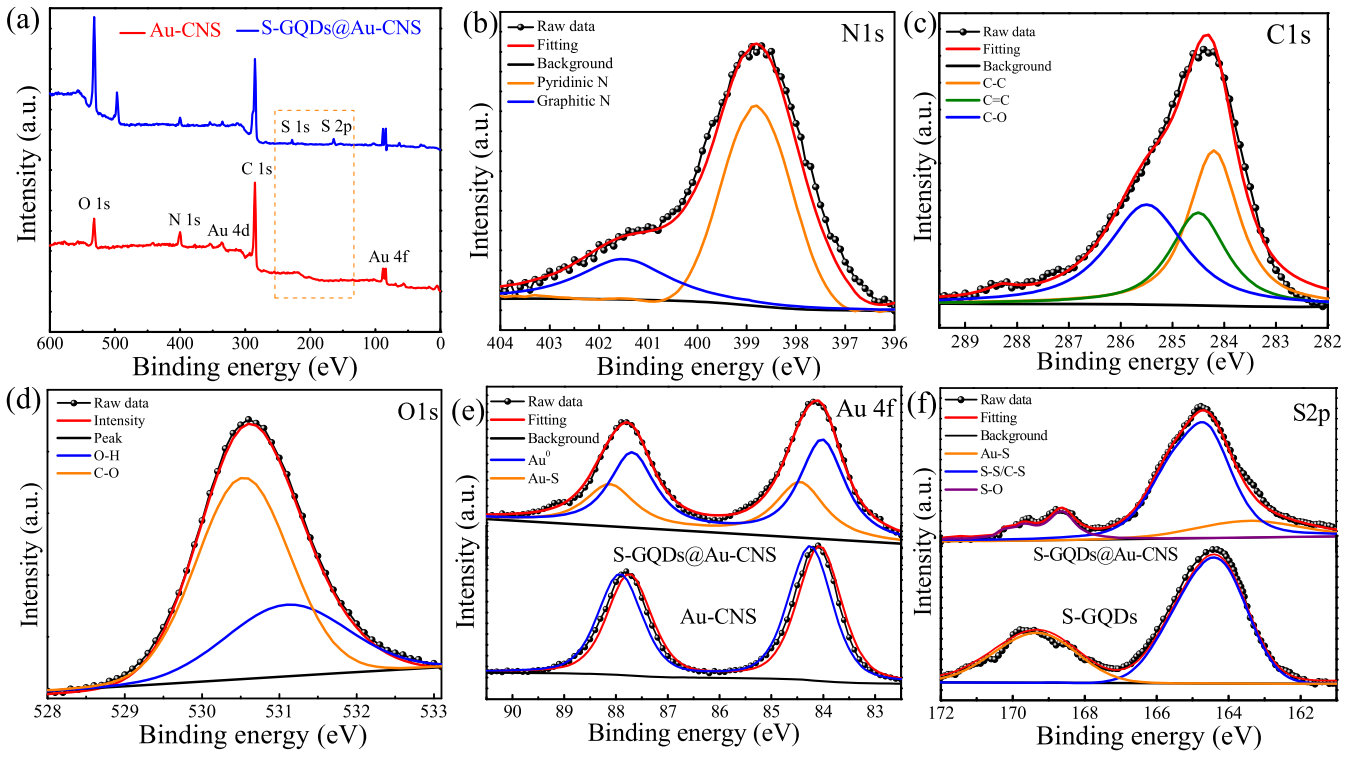

Fig. 2. The (a) XPS survey spectra of as-synthesized Au–CNS and S-GQDs@Au–CNS, the deconvoluted XPS of (b) N 1s, (c) C 1s, and (d) O 1s spectra of Au–CNS, (e) Au 4f, and (f) S 2p peaks of Au–CNS and S-GQDs@Au–CNS nanocomposites.

2.6. Preparation of the sensor electrode

The biosensing electrode was prepared by drop-casting the nanocomposite onto the glassy carbon electrode (GCE). Prior to the preparation of the sensor electrode, GCE was polished with 1.0 and 0.3 μm alumina powders first and then rinsed with DI water. To fabricate the electrode used in this work, 5 μL of 5.0 mg mL^{-1} Ang-2 conjugated S-GQDs@Au–CNS NPs solution was drop-casted on the polished GCE electrode to prepare the sensing probe and stored at 4 °C for further usage.

2.7. Glioma cell sensing

Prior to the biosensing, 0.1 M phosphate buffer saline (PBS) at pH 7.4 was used to dilute the glioma cell solution. The glioma cell solution was then added onto the surface of GCE||CNS–Au@S-GQDs/Ang-2 electrode and incubated for 10 min. The unbound cells were removed from the electrode by gently washing with deionized water. Then, the impedance was measured in PBS buffer using Autolab electrochemical impedance spectrometer (EIS) in the frequency range of 100 kHz to 10 mHz at an amplitude of 2 mV.

To examine the applicability of the sensing system for real-time biomedical application, the GCE||CNS–Au@S-GQDs/Ang-2 electrode was applied using the standard addition method to determine the glioma cells in sophisticated biological sample matrix using 10% human serum as the detection medium. Various known concentrations of the glioma cells were spiked into diluted human serum solutions. Glioma cells are detected in the human serum samples using the potential EIS sensing mode following procedure same as in the buffer solution.

3. Results and discussion

3.1. Working principle

Scheme 1b shows the detection principal of the newly developed pulse-induced impedimetric biosensor for robust and ultrasensitive detection of glioma cells using S-GQDs@Au–CNS nanocomposites as the electrode matrix. The Ang-2/S-GQDs@Au–CNS electrode can specifically recognize the glioma cells, leading to the decrease in conductivity after the formation of glioma cells–angiopep bioconjugate on the surface of S-GQDs@Au–CNS. Moreover, the application of the external potential during the biosensing process provides a strategy to amplify the detection sensitivity of the glioma cells biosensing as well as to achieve the low detection limit. The external pulse can influence the surface permeability as well as cell membrane expansion of cancer cells (Yarmuch et al., 2014), which facilitates the increase in the probability of binding cancer cells onto the Ang-2/S-GQDs@Au–CNS electrode, resulting in the enhancement of sensitivity and selectivity toward glioma cell detection by S-GQDs@Au–CNS.

3.2. Characterization of S-GQD@Au–CNS nanosensing probe

To establish the biosensing platform, the size and morphology of S-GQDs are initially characterized. The TEM image in Fig. 1a shows the 5–10 nm S-GQDs in spherical shape with homogeneous distribution. The in-plane lattice spacing of 0.21 nm, which is ascertained as the (100) graphene plane, confirm the formation of S-GQDs with sp^2 graphitic crystal phase (Fig. 1b) (Ganganboina et al., 2017a, 2017b). The histogram in Fig. 1c signifies the uniform distribution range of 4–11 nm with an average diameter of 7 nm, which is in good agreement with the recently reported diameter range of S-GQDs (Anh and Doong, 2018; Anh et al., 2019; Tran and Doong, 2019).

Gold nanoparticles decorated carbon nanospheres (Au–CNS) are prepared by a dual surfactant templating method coupled with coordination bonding between metal ions and amine functional groups onto CNS, which can reduce Au^{3+} ions to AuNPs by thermal reduction. The TEM images in Fig. 1d shows the monodispersed AuNPs onto carbon nanospheres (Au–CNS). A previous study indicated that the CNS pore channels have a dominant role in acting as nano-containers to facilitate the development of AuNP during thermal reduction, leading to the

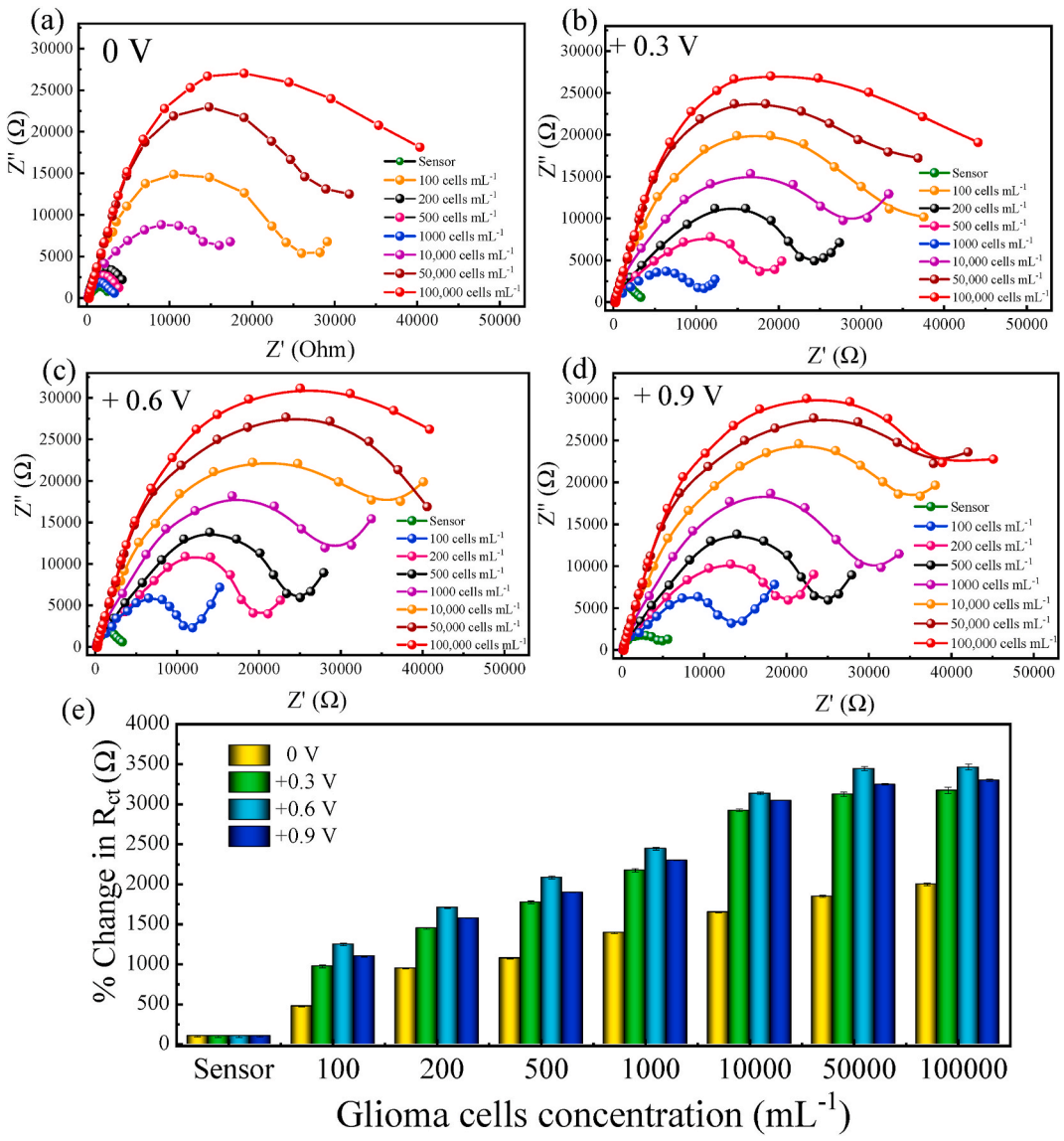

Fig. 3. The electrochemically impedimetric performances on the GCE||CNS–Au@S-GQDs/Ang-2 biosensor electrode during the detection of glioma cells over various electric pulses at (a) 0, (b) +0.3, (c) +0.6 and (d) +0.9 V, and (e) comparative diagram of percentage change in charge transfer resistance (R_{ct}) values in the presence of different external potentials.

creation of ultra-small and uniform AuNPs (Yang et al., 2016). The aminophenol resin precursor supplies amine functional groups for metal ion coordination, facilitating the interface between the carbon precursor and Au NPs. In this study, the hexagonal lattice is clearly seen in the fast Fourier transform pattern (Fig. 1e), which indicates the (111) AuNP orientation (Chowdhury et al., 2018b). The histogram displayed in Fig. 1f signifies that the mean diameter of AuNP is 10 nm with a particle size distribution of 6–14 nm. In addition, the thermal reduction facilitates the reduction of Au ions within the nanosphere, which is favourable for the formation of uniformly dispersed AuNPs embedded on CNS.

The S-GQDs can be easily deposited onto the Au–CNS by Au-thiol chemistry. After the thiol conjugation between S-GQDs and Au–CNS, the Au–CNS nanosphere still maintains its integrity in morphology and dispersivity (Fig. 1g). As illustrated in HRTEM image (Fig. 1h), the fringe pattern of S-GQDs@Au–CNS nanocomposites clearly shows two different patterns of S-GQDs and AuNPs. The AuNP lattice spacing of 0.24 nm (Fig. 1i) can be readily distinguished from the S-GQD lattice spacing of 0.21 nm, which is the characteristic fringe of the graphite lattice.

The structural property of the S-GQDs@Au–CNS nanocomposites is identified by XRD. As shown in Fig. 1j, the XRD patterns at 38.1°, 44.2°, 64.4°, and 77.6° 2θ, which correspond to (111), (200), (220), and (311) planes, respectively, are the characteristic peaks of AuNPs (Ganganboina and Doong 2019). A broad peak at 24° 2θ is the amorphous nature of carbon from CNS. After the formation of S-GQDs@Au–CNS, no observable shift in the Au peak positions is observed even though the intensity of the peaks decreases. The binding of S-GQDs onto the Au–CNS nanocomposites via Au-thiol interaction has little effect on the AuNP crystal patterns, and, therefore, the electroactive nature of the metallic Au can thus be maintained for electrochemical sensing in the nanocomposite. Furthermore, the TGA is performed in air to estimate the amount of AuNPs and S-GQDs in S-GQDs@Au–CNS based nanocomposites. The total weight loss of synthesized Au–CNS is 40.8 wt% and S-GQDs@Au–CNS is 36.2 wt%. The weight loss of Au–CNS between 30 and 200 °C is attributed to the removal of physically adsorbed water molecules. The weight loss majorly occurs in the temperature range of 450–700 °C, which is mainly contributed from the decomposition of CNS. Moreover, an additional weight loss of 4.6% at 350–550 °C is noticed for S-GQDs@Au–CNS in comparison with as-synthesized Au–CNS, which means that the added weight percentage of S-GQDs in

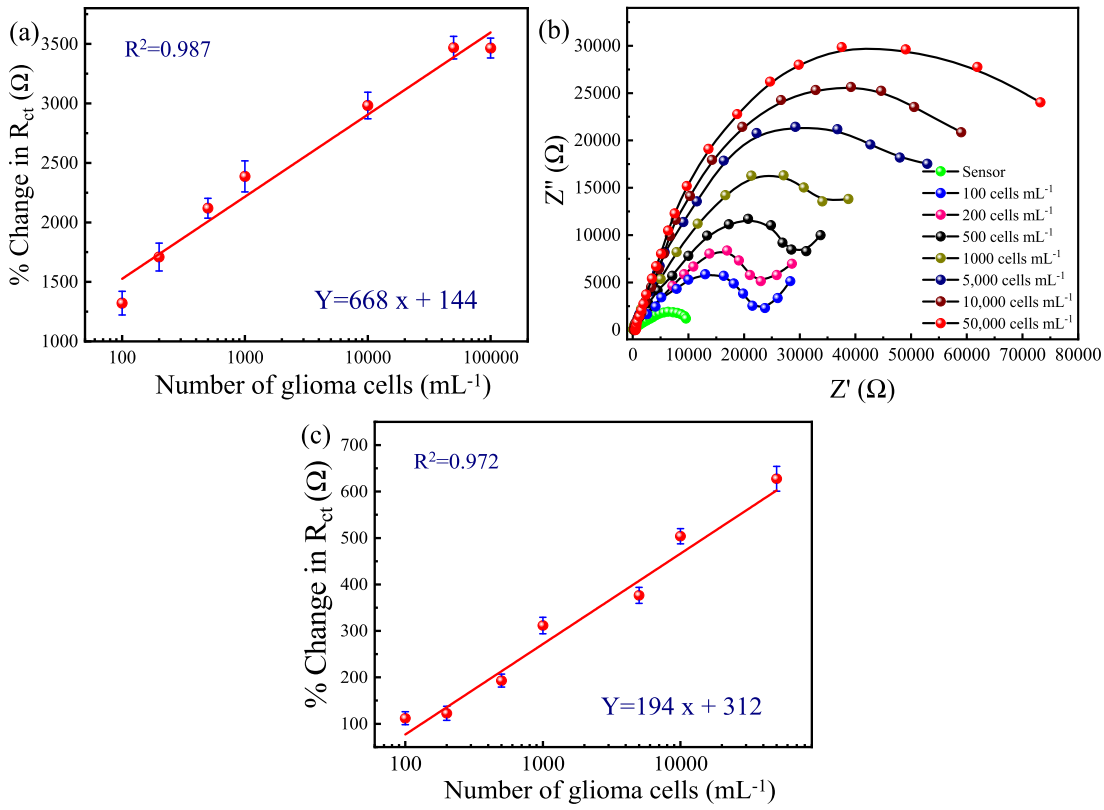

Fig. 4. The (a) calibration line obtained from change in R_{ct} vs glioma cells concentration, (b) Nyquist plot of GCE||CNS–Au@S-GQDs/Ang-2 sensor at various concentration of glioma cells in human serum, and (c) calibration line obtained from the change in R_{ct} vs glioma cells concentration.

the S-GQDs@Au–CNS nanocomposites is around 4.6%.

XPS is conducted to evaluate the change in elemental species of Au–CNS before and after the attachment of S-GQDs. The survey spectrum of Au–CNS exhibits peaks of O 1s (531 eV), N 1s (400 eV), Au 4 d (335 and 354 eV), C 1s (284 eV) and Au 4f (85.8 and 83.9 eV) (Fig. 2a). Two additional peaks at 228 eV (S 1s) and 162 eV (S 2p) appear after the attachment to S-GQDs, which are the typical S peaks from the S-GQDs. The deconvolution of N 1s spectrum of Au–CNS (Fig. 2b) signifies the presence of graphitic (401.5 eV) and pyridinic (398.9 eV) N elements, presumably attributed to the NH_2 functional groups in the CNS. The deconvoluted C1s spectrum of Au–CNS exhibits three peaks at 284.1 (C–C), 284.2 (C═C) and 285.5 eV (C–O) (Fig. 2c) (Feng et al., 2019). Moreover, the peak at 530.3 eV in the deconvoluted spectrum of O 1s is attributed to the C–O functional group, while 531.1 eV can be assigned to hydroxyl groups (O–H) of Au–CNS (Fig. 2d).

To further evaluate the Au-thiol linkage of S-GQDs to Au–CNS nanocomposites, the S 2p and Au 4f peaks of Au–CNS and S-GQDs@Au–CNS are deconvoluted. As displayed in Fig. 2e, the Au 4f exhibits peak at 84.3 eV in Au–CNS, and then marginally shifts to 84.0 eV after the linkage of S-GQDs with Au–CNS, likely due to the fact that the sulfur elements next to the AuNPs produce higher electronegative environment in comparison to the pure Au–CNS. After the deconvolution of Au 4f peak in Au–CNS, the Au^0 peak is the only dominant species. However, an additional peak at 84.4 eV in the S-GQDs@Au–CNS appears, confirming the formation of Au–S bonds. Moreover, the Au–S linkage is also confirmed from the deconvolution of S 2p spectra of S-GQDs and S-GQDs@Au–CNS (Fig. 2f). The deconvoluted peak at 162.4 eV is contributed from the formation of Au–S bond between Au–CNS and S-GQDs (Anh and Doong, 2018), which corroborates the formation of S-GQDs@Au–CNS.

3.3. Optimization of electrochemical performance of S-GQD@Au–CNS electrode

The influence of experimental parameters including pH, concentration of Ang-2, and added amounts of S-GQD@Au–CNS on the electrochemical performance of GCE||CNS–Au@S-GQDs/Ang-2 biosensor electrode was further optimized. As shown in Fig. S1a (Supplementary data), the R_{ct} increases with the increase in Ang-2 concentration from 1 to 10 μg mL^{-1} and no further change in impedance is observed when the loading is higher than 10 μg mL^{-1}. This is mainly attributed to the fact that low concentration of Ang-2 at 1–10 μg mL^{-1} increases the resistance and then reaches the saturation at the Ang-2 loading of 10 μg mL^{-1}, which signifies that 10 μg mL^{-1} Ang-2 is the optimal concentration for biosensing of glioma cells.

The added amount of S-GQDs@Au–CNS onto the electrode may change the film thickness of sensing probe to influence the impedance, and, therefore, the concentration of S-GQDs@Au–CNS deposited onto GCE was further optimized. As shown in Fig. S1b (Supplementary data), the detection performance of the electrode increases when the S-GQDs@Au–CNS concentration increases from 1 to 5 mg mL^{-1} and then decreases upon the increase in loading concentration to 7 mg mL^{-1}. It is noteworthy that the particle size of the as-prepared CNS–Au@S-GQDs is in the range of 250–300 nm, and the highly added amount of CNS–Au@S-GQDs may produce a thick film on the surface of GCE electrode during the drop-casting procedure, which may result in the decrease in electron transfer and the increase in resistance. Therefore, 5 mg mL^{-1} S-GQDs@CNS–Au is used for the further experiments. Moreover, the pH of electrolyte would affect the efficiency of immobilization and bioactivity of biotarget. Fig. S1c (Supplementary data) shows the effect of electrolyte pH on the response of developed biosensor to glioma cells at 1000 cells mL^{-1}. It is clear that the response of GCE||CNS–Au@S-GQDs/Ang-2 electrode increases upon increasing the pH from pH 5.5 to 7.5, and then decreases again at high pH value of 8.5, clearly indicating

that the pH 7.5 is the optimal electrolyte pH and is then used for further experiments for glioma cell detection.

3.4. Effect of electrical pulse on impedimetric sensing response

After the successful characterization of Au–CNS and S-GQD@Au–CNS, the nanocomposite was coated onto the surface of GCE to form the electrochemical biosensors. Fig. 3 shows the Nyquist plots of the GCE||CNS–Au@S-GQDs/Ang-2 sensor electrode incubated with 100–100,000 cells mL^{-1} glioma cells in a frequency range of 100 kHz–10 mHz. The detection of glioma cells is based on the increase in impedance response to the GCE||CNS–Au@S-GQDs/Ang-2 sensor electrode when gliomas cells are bioconjugated with Ang-2 on the S-GQDs/Au–CNS surface. The diameter of semicircle in Nyquist plot increases after the addition of glioma cells because of the increase in charge transfer resistance (R_{ct}) at the electrode-electrolyte interface caused by the attachment of glioma cells. As shown in Fig. 3a, the Nyquist plots clearly show that the charge transfer resistance increases progressively upon the addition of glioma cells from 1000 to 100,000 cells mL^{-1}, which is in good accordance with the recent works (Chowdhury et al., 2018a; Hassan and DeRosa, 2020; Sun et al., 2019). It is noteworthy that the change in impedance of GCE||CNS–Au@S-GQDs/Ang-2 sensor electrode is less profound when the concentration of glioma cells is less than 1000 cells mL^{-1}, presumably due to the low sensitivity toward impedance measurement.

To achieve the highly sensitive performance on glioma cell detection, an external pulse is applied during the attachment of glioma cells to the GCE||CNS–Au@S-GQDs/Ang-2 biosensing electrode. The hypothesis is based on the fact that surface permeability and cell membrane expansion correlate strongly with the applied pulse intensity during the electroporation-mediated process (Xing et al., 2007; Yarmush et al., 2014). To examine the optimal parameters for biosensing of glioma cells, various electrical pulse intensities at 0, +0.3, +0.6 and + 0.9 V are investigated. Fig. 3b–d shows the impedimetric spectra of GCE||CNS–Au@S-GQDs/Ang-2 sensor electrode in the presence of 100–100,000 cells mL^{-1} glioma cells at 0.3–0.9 V. By comparing the change in impedance with the applied external pulse as the function of the glioma cells (Fig. 3e), it is clear that the employment of external potential significantly enhances the impedance sensitivity of GCE||CNS–Au@S-GQDs/Ang-2 at low glioma cell concentrations up to 100 cells mL^{-1}. However, the sensitivity declines at high concentrations of glioma cells (50,000 to 100,000 cells mL^{-1}) when the pulse of +0.9 V is applied. This may be due to the possible damage to the S-GQDs@Au–CNS architecture at high potential (Paganin-Gioanni et al., 2011). In addition, the large transmembrane voltage results in the irreversible electroporation in tumors, leading to the increase in cell conductivity (Granot et al., 2009). Therefore, it can be concluded that the external pulse at +0.6 V during the attachment of glioma cells is the most suitable condition for the detection of glioma cells in a wide range of concentrations.

The R_{ct} before the loading of glioma cells is low because of the good electron transfer between the electrolyte and the surface of GCE||CNS–Au@S-GQDs/Ang-2 electrode. Upon the addition of glioma cells, the conducting surface of S-GQDs and Au–CNS is covered with the significant number of non-conducting glioma cells, resulting in the increase in R_{ct}. The difference in R_{ct} values of the GCE||CNS–Au@S-GQDs/Ang-2 electrode after incubation with glioma cells is used as the analytical signal. The calibration curve obtained by GCE||CNS-AuNPs@ S-GQDs/Ang-2 sensor electrode using the change in impedance response measured by applying electric pulse of +0.6 V during the addition of glioma cells solution is shown in Fig. 4a. It is apparent that the change in R_{ct} increases proportionally to the glioma cells concentration and a good linear correlation between the change in R_{ct} and glioma cells concentration in the range of 100–100,000 cells mL^{-1} is obtained. Moreover, the limit of detection (LOD), estimated by $3\sigma/S$ where σ represents the standard deviation of the lowest signal and S represents the slope of obtained linear calibration curve (Ganganboina and Doong, 2018a), is calculated to be 40 cells mL^{-1}.

Results obtained in this study explicitly demonstrate that the application of electric pulse increases the sensitivity of the sensor electrode. This enhancement is mainly due to that fact that the high electron transfer capability of the fabricated electrode is primarily attributed from the S-GQDs with its unique optoelectronic property, which is inherited to the S-GQDs@Au–CNS nanocomposites. In this study, the excess amounts of S-GQDs are added to allow the maximum attachment of S-GQDs onto the Au–CNS during the synthesis process and the attached amount of S-GQDs is highly dependent onto the amount of Au on the surface of Au–CNS. Although the S-GQDs content can be increased by the increase in Au amounts or by stacking of S-GQDs, the morphology and electrochemical performance of Au–CNS will be changed and then alter the electrochemical performance because of the increase in thickness and stacking effect of S-GQDs. In addition, the Au–CNS usually exhibits a superior conductivity and high surface area (Chang and Doong, 2019). Therefore, the uniform dispersion of AuNPs on the CNS surface provides numerous active sites for successful attachment of S-GQDs by Au-thiol linkage. Furthermore, with the different reaction sites of Au-thiol interaction and the conjugation of Ang-2 to the S-GQDs, the S-GQD@Au–CNS provides proficient active sites to anchor Ang-2. In addition to the electronic structure of the electrode matrix, the electric pulse increases the exposure of the surface of cancer cells, which allows the increasing opportunity for glioma cells to bind to Ang-2-modified S-GQDs (Breton and Mir, 2012). Silve et al. (2012) have demonstrated that the application of electric pulse can create new pores or defects on the cell membrane of lung cell line, allowing the uptake of external molecules into the cytoplasm. In addition, Paganin-Gioanni et al. (2011) have applied the external electric pulse to deliver siRNA into murine melanoma cells, and found that the applied electrical field is effective on both the permeability of the plasma cell membrane and the dragging of the siRNA molecules into the cytoplasm. Table S1 (Supplementary data) summarizes the analytical performance of cancer cell detection by different electrochemically sensing probes. The wide dynamic range with low LOD of the developed impedimetric biosensor for glioma cells detection is comparable with or even superior to the recently developed sensing methods (Chowdhury et al., 2018a; Guo et al., 2020; Yaman et al., 2019; Zhou et al., 2019). In comparison to these reports, we presume that the applied electric pulse might extend the glioma cell surfaces in a very limited scale, thus providing more visible surface markers to Ang-2.

3.4. Glioma cells detection in human serum

To evaluate the matrix effect on the developed biosensor for cancer cell detection, 10% human serum is used as sophisticated biological medium. Initially, the impedimetric response of GCE||CNS–Au@S-GQDs/Ang-2 sensor is measured in blank human serum solution which is used as the baseline for further analysis. As shown in Fig. 4b, the R_{ct} value of 9542 Ω for Au@S-GQD/Ang-2 biosensor in human serum is observed, indicating the presence of unspecified interaction of the matrix proteins with sensor electrode. To evaluate the feasibility of glioma cell detection in the complex matrix sample, various concentrations of glioma cells were spiked into the human serum. A similar responsive pattern in the human serum detection, i.e. the R_{ct} increases upon the increase in glioma cell concentration, is observed in comparison with the glioma cell detection in PBS, evincing the applicability of the developed biosensor for clinical sample monitoring. In addition, the calibration curve obtained for glioma cells detection using 10% human serum is shown in Fig. 4c. A good linear relationship between R_{ct} and glioma cell concentration with r^2 of 0.972 is observed. It is noteworthy that the slope of calibration curve in the complex matrix sample is flat in comparison with the response in PBS buffer, presumably because of the interference of other biomolecules in the complex serum matrix to the impedance of the GCE||CNS–Au@S-GQDs/Ang-2. Although the

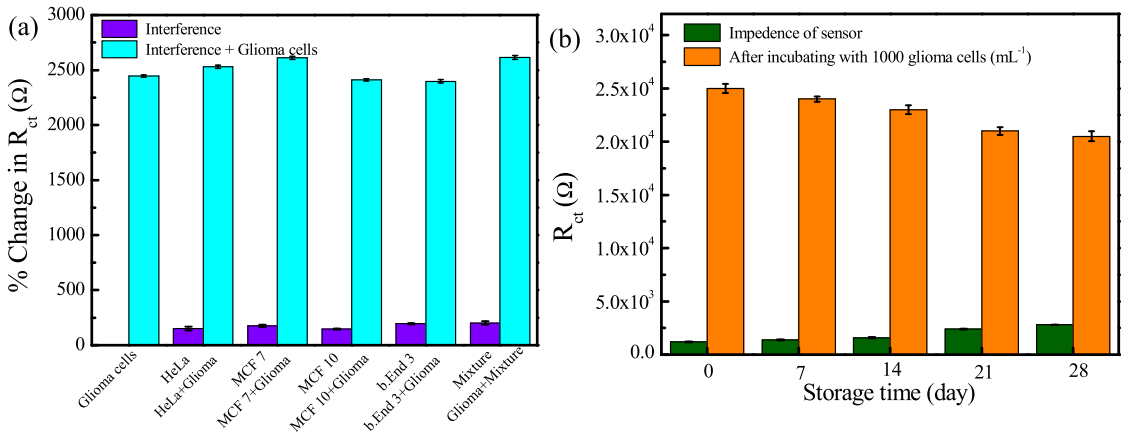

Fig. 5. The (a) specificity and (b) stability of GCE||CNS–Au@S-GQDs/Ang-2 biosensor toward glioma cell detection in human serum.

proposed biosensor is affected by complex matrix in serum, the excellent linearity signifies its good applicability for the detection of 100–50,000 cells mL^{-1} glioma cells in human serum samples.

A significant factor in the practical use of the biosensor is its specificity. The Ang-2 conjugates majorly interact with the membrane receptor molecule of glioma cells governing the specificity of the biosensor electrode. To evaluate the selectivity of the GCE||CNS–Au@S-GQDs/Ang-2 biosensor, various cells like MCF-7, MCF-10, and HeLa at 10,000 cells mL^{-1} are used as interferences through the comparison of the impedance response to glioma cells. Fig. 5a shows the impedimetric response of GCE||CNS–Au@S-GQDs/Ang-2 sensor to several interferences and glioma cells. The small change in R_{ct} (145–200 Ω) after the addition of interferences elaborates that the interaction of interferences with GCE||CNS–Au@S-GQDs/Ang-2 sensor electrode is small. When interferences are combined with glioma cells, however, the R_{ct} increases dramatically to 2398–2615 Ω. In addition, the R_{ct} increases from 2446 ± 18 Ω for glioma cells only to 2615 ± 24 Ω for mixture containing glioma cells and all other interferences, corroborating the high selectivity of GCE||CNS–Au@S-GQDs/Ang-2 sensor towards glioma cells detection. The reproducibility of the as-prepared sensor was further evaluated by fabricating five different electrodes for the detection of 1000 glioma cells mL^{-1}. Fig. S2 (Supplementary data) shows the response of R_{ct} to the detection of 1000 cells mL^{-1} glioma cells by five different electrodes. The measured impedances of the as-prepared electrode are in the range of 2352–2568 Ω, which means that the measured concentration of glioma cells is in the range of 962–1015 cells mL^{-1} with an average of 995 cells mL^{-1}. In addition, the precision of the measured concentration after five replicates is only 3.8%. Since the added amount of glioma cell is 1000 cells mL^{-1}, the average value of 995 cells mL^{-1} with relative standard deviation of 3.8% signifies the accuracy and excellent reproducibility of immunosensor developed in this study.

The stability of the prepared GCE||CNS–Au@S-GQDs/Ang-2 biosensor is also evaluated by storing the prepared sensor electrodes at 4 °C for 4 weeks, and the response of the GCE||CNS–Au@S-GQDs/Ang-2 to glioma cells was measured periodically. As shown in Fig. 5b, the impedimetric response of the GCE||CNS–Au@S-GQDs/Ang-2 to glioma cells remains stable after 14 d of storage, and the recovery was determined to be 94 ± 3%. After the 21- and 28-day storage, the electrode can retain the originally impedimetric response of 86 ± 4% and 84 ± 4%, respectively. This excellent long-term stability makes S-GQD@Au–CNS nanocomposite a promising material for biosensing application with long-term stability for the detection of glioma cells.

4. Conclusions

In this study, we have developed the electrochemical impedimetric biosensor by using Ang-2/S-GQDs@Au–CNS nanocomposite as the sensing probe for ultrasensitive detection of glioma cells in PBS and human serum. The developed biosensing probe, Ang-2-S-GQDs@Au–CNS, exhibits the specific binding ability of Ang-2 toward LRP1 receptors on the glioma cell surface, making Ang-2-S-GQDs@Au–CNS nanocomposite a major advantage over other reported sensing techniques. In addition, the electrochemically impedimetric process has been engineered by the use of the external electrical pulse at 0.6 V during the biosensing process. The developed GCE||CNS–Au@S-GQDs/Ang-2 biosensor exhibits its superiority to detect glioma cells. The pulse-induced mechanism for impedimetric sensing increases the sensitivity of the sensor in detecting the glioma cells, and a wide linear range from 100 to 100,000 cells mL^{-1} with a LOD of 40 cells mL^{-1} is observed. Moreover, an excellent selectivity with long-term storage stability of the developed biosensing probe for glioma cells detection is observed. Results clearly demonstrates that the superior analytical performance of the developed S-GQDs@Au–CNS biosensing probe in both PBS and human serum matrix signifies the feasibility of practical application, which can facilitate the development of ultrasensitive and potent impedance-based sensors for cancer cells detection.

CRediT authorship contribution statement

Akhilesh Babu Ganganboina: and, Conceptualization, Methodology, Software, Formal analysis, Data curation, Visualization. **Naresh Kumar Dega:** and, Software, Formal analysis, Data curation, Visualization. **Hai Linh Tran:** Validation, Formal analysis, Data curation, Visualization. **Win Darmonto:** and, Validation, Resources, Data curation, Writing – original draft, preparation, Writing – review & editing, Project administration. **Ruey-An Doong:** Conceptualization, Methodology, Validation, Resources, Writing – original draft, preparation, Writing – review & editing, Supervision, Project administration, Funding acquisition.

Declaration of competing interest

The authors declare that they have no known competing financial interests or personal relationships that could have appeared to influence the work reported in this paper.

Acknowledgement

The authors thank the Ministry of Science and Technology (MOST)), Taiwan for financial support under grant Nos. MOST 108-2113-M-007-021-MY3. A.B.G. is acknowledged to the MOST, Taiwan for financial support and sincerely thanks the Japan Society for the Promotion of Science (JSPS) for a postdoctoral fellowship (Grant No. 19F19064).

Appendix A. Supplementary data

Supplementary data to this article can be found online at https://doi.org/10.1016/j.bios.2021.113151.

References

Ahmadi, N., Bagherzadeh, M., Nemati, A., 2020. Biosens. Bioelectron. 151, 111977.
Anh, N.T.N., Doong, R.A., 2018. ACS Appl. Nano Mater. 1 (5), 2153–2163.
Anh, N.T.N., Chang, P.Y., Doong, R.A., 2019. RSC Adv. 9, 26588–26597.
Bidram, E., Esmaeili, Y., Ranji-Burachaloo, H., Al-Zaubai, N., Zarrabi, A., Stewart, A., Dunstan, D.E., 2019. J. Drug Deliv. Sci. Technol. 54, 101350.
Breton, M., Mir, L.M., 2012. Bioelectromagnetics 33 (2), 106–123.
Chang, P.Y., Doong, R.A., 2019. J. Alloys Compd. 775, 214–224.
Chowdhury, A.D., Ganganboina, A.B., Park, E.Y., Doong, R.A., 2018a. Biosens. Bioelectron. 122, 95–103.
Chowdhury, A.D., Ganganboina, A.B., Tsai, Y.C., Chiu, H.C., Doong, R.A., 2018b. Anal. Chim. Acta 1027, 109–120.
Dutta Chowdhury, A., Ganganboina, A.B., Nasrin, F., Takemura, K., Doong, R.A., Utomo, D.I.S., Lee, J., Khoris, I.M., Park, E.Y., 2018. Anal. Chem. 90 (21), 12464–12474.
Feng, S., Liu, Z., Yu, Q., Zhuang, Z., Chen, Q., Fu, S., Zhou, L., Mai, L., 2019. ACS Appl. Mater. Interfaces 11 (4), 4011–4016.
Ganganboina, A.B., Chowdhury, A.D., Doong, R.A., 2017a. Electrochim. Acta 245, 912–923.
Ganganboina, A.B., Chowdhury, A.D., Khoris, I.M., Nasrin, F., Takemura, K., Hara, T., Abe, F., Suzuki, T., Park, E.Y., 2020. Biosens. Bioelectron. 157, 112169.
Ganganboina, A.B., Doong, R.A., 2018a. Sens. Actuators, B 273, 1179–1186.
Ganganboina, A.B., Doong, R.A., 2018b. Microchim. Acta 185 (11), 526.
Ganganboina, A.B., Doong, R.A., 2019. Sci. Rep. 9 (1), 1–11.
Ganganboina, A.B., Doong, R.A., 2020. Environ. Sci.: Nano 7, 228–237.
Ganganboina, A.B., Dutta Chowdhury, A., Doong, R.A., 2017b. ACS Sustain. Chem. Eng. 5 (6), 4930–4940.
Guo, C., Li, Z., Duan, F., Zhang, Z., Marchetti, F., Du, M., 2020. J. Mater. Chem. B 8 (43), 9951–9960.
Hassan, E.M., DeRosa, M.C., 2020. Trends Anal. Chem. 124, 115806.
Hu, L.S., Brat, D.J., Bloch, O., Ramkissoon, S., Lesser, G.J., 2020. Am. Soc. Clin. Oncol. Educ. Book 40, 1–12.
Huang, S., Li, J., Han, L., Liu, S., Ma, H., Huang, R., Jiang, C., 2011. Biomaterials 32 (28), 6832–6838.
Khongkow, M., Yata, T., Boonrungsiman, S., Ruktanonchai, U.R., Graham, D., Namdee, K., 2019. Sci. Rep. 9 (1), 1–9.
Kumar, A., Pathak, P.K., Prasad, B.B., 2019. ACS Appl. Mater. Interfaces 11 (17), 16065–16074.
Li, Y., Hu, M., Huang, X., Wang, M., He, L., Song, Y., Jia, Q., Zhou, N., Zhang, Z., Du, M., 2020. Sensor. Actuator. B Chem. 306, 127608.
Mansuriya, B.D., Altintas, Z., 2020. Materials 13 (1), 96.
Miao, X., Wen, S., Su, Y., Fu, J., Luo, X., Wu, P., Cai, C., Jelinek, R., Jiang, L.-P., Zhu, J.-J., 2019. Anal. Chem. 91 (11), 7295–7303.
Paganin-Gioanni, A., Bellard, E., Escoffre, J.-M., Rols, M.-P., Teissie, J., Golzio, M., 2011. Proc. Natl. Acad. Sci. U.S.A. 108 (26), 10443–10447.
Prager, B.C., Bhargava, S., Mahadev, V., Hubert, C.G., Rich, J.N., 2020. Trends in Cancer 6 (3), 223–235.
Silve, A., Leray, I., Mir, L.M., 2012. Bioelectrochemistry 87, 260–264.
Song, Z., Chen, M., Ding, C., Luo, X., 2020. Anal. Chem. 92, 5795–5802.
Sun, D., Lu, J., Zhang, L., Chen, Z., 2019. Anal. Chim. Acta 1082, 1–17.
Tran, H.L., Doong, R.A., 2019. Anal. Methods 11, 4421–4430.
Tom, M.C., Cahill, D.P., Buckner, J.C., Dietrich, J., Parsons, M.W., Yu, J.S., 2019. Am. Soc. Clin. Oncol. Educ. Book 39, 133–145.
Wang, M., Yin, H., Zhou, Y., Sui, C., Wang, Y., Meng, X., Waterhouse, G.I., Ai, S., 2019. Biosens. Bioelectron. 128, 137–143.
Wang, X., Liu, G., Chen, N., Wu, J., Zhang, J., Qian, Y., Zhang, L., Zhou, D., Yu, Y., 2020a. ACS Appl. Mater. Interfaces 12 (10), 12143–12154.
Wang, X., Wei, F., Yan, S., Zhang, H., Tan, X., Zhang, L., Zhou, G., Cui, L., Li, C., Wang, L., 2014. Biosens. Bioelectron. 54, 55–63.
Wang, Y., Zhao, B., Chen, W., Liu, L., Chen, W., Zhou, L., Kong, Z., Dai, C., Wang, Y., Ma, W., 2020b. Aging Dis 11 (2), 448–461.
Xing, Y., Chaudry, Q., Shen, C., Kong, K.Y., Zhau, H.E., Chung, L.W., Petros, J.A., O'regan, R.M., Yezhelyev, M.V., Simons, J.W., 2007. Nat. Protoc. 2 (5), 1152–1165.
Xue, G., Yu, S., Qiang, Z., Xiuying, L., Jiangrong, L., 2020. Anal. Chim. Acta 1108, 46–53.
Yang, J., Shi, Z., Liu, R., Wu, Y., Zhang, X., 2020. Theranostics 10 (7), 3223–3239.
Yang, T., Ling, H., Lamonier, J.-F., Jaroniec, M., Huang, J., Monteiro, M.J., Liu, J., 2016. NPG Asia Mater. 8 (2), e240.
Yang, T., Liu, J., Zhou, R., Chen, Z., Xu, H., Qiao, S.Z., Monteiro, M.J., 2014. J. Mater. Chem. 2 (42), 18139–18146.
Yaman, Y.T., Akbal, O., Abaci, S., 2019. Biosens. Bioelectron. 132, 230–237.
Yarmush, M.L., Golberg, A., Serša, G., Kotnik, T., Miklavčič, D., 2014. Annu. Rev. Biomed. Eng. 16, 295–320.
Zhou, N., Su, F., Li, Z., Yan, X., Zhang, C., Hu, B., He, L., Wang, M., Zhang, Z., 2019. Microchim. Acta 186 (2), 1–10.